This is the accepted manuscript made available via CHORUS. The article has been published as:

Collective excitations in the tetravalent lanthanide honeycomb antiferromagnet math xmlns="http://www.w3.org/1998/Math/MathML">mrow>msub>mi>Na/mi>mn>2/mn>/msub>mi>Pr/mi>msub>mi mathvariant="normal">O/mi>mn>3/mn>/msub>/mrow>/math>

M. J. Daum, A. Ramanathan, A. I. Kolesnikov, S. Calder, M. Mourigal, and H. S. La Pierre

Phys. Rev. B **103**, L121109 — Published 12 March 2021

DOI: 10.1103/PhysRevB.103.L121109

Collective excitations in the tetravalent lanthanide honeycomb antiferromagnet, Na_2PrO_3

M. J. Daum,[1,*] A. Ramanathan,[2,*] A. I. Kolesnikov,[3] S. Calder,[3] M. Mourigal,[1,†] and H. S. La Pierre[2,4,‡]

[1] *School of Physics, Georgia Institute of Technology, Atlanta, GA 30332, USA*
[2] *School of Chemistry and Biochemistry, Georgia Institute of Technology, Atlanta, GA 30332, USA*
[3] *Neutron Scattering Division, Oak Ridge National Laboratory, Oak Ridge, TN 37831, USA*
[4] *Nuclear and Radiological Engineering and Medical Physics Program, School of Mechanical Engineering, Georgia Institute of Technology, Atlanta, GA 30332, USA*

(Dated: February 24, 2021)

Thermomagnetic and inelastic neutron scattering measurements on Na_2PrO_3 are reported. This material is an antiferromagnetic honeycomb magnet based on the tetravalent lanthanide Pr^{4+} and has been proposed to host dominant antiferromagnetic Kitaev interactions. These measurements reveal magnetic fluctuations in Na_2PrO_3 below an energy of 2 meV as well as crystal-field excitations around 230 meV. The latter energy is comparable to the scale of the spin-orbit interaction and explains both the very small effective moment of around 1.0 μ_B per Pr^{4+} and the difficulty to uncover any static magnetic scattering below the ordering transition at $T_N = 4.6$ K. By comparing the low-energy magnetic excitations in Na_2PrO_3 to that of the isostructural spin-only compound, Na_2TbO_3, a microscopic model of exchange interactions is developed that implicates dominant and surprisingly large Heisenberg exchange interactions $J \approx 1.1(1)$ meV. Although antiferromagnetic Kitaev interactions with $K \leq 0.2J$ cannot be excluded, the inelastic neutron scattering data of Na_2PrO_3 is best explained with a $\Delta = 1.22$ easy-axis XXZ exchange anisotropy.

Frustrated quantum magnets have been proposed as a platform to realize quantum spin-liquids (QSLs) and other exotic forms of magnetic matter [1, 2]. In QSLs, quantum fluctuations are so strong that spins remain disordered for temperatures well below the average interaction scale between spins and become entangled. Geometrically frustrated lattices featuring lanthanide ions have gained much recent attention, including the triangular, kagome, and pyrochlore systems [3–8]. An alternative realization of a QSL (with an exact solution) was proposed by Kitaev based on $S = 1/2$ moments on a honeycomb lattice with bond-dependent Ising-like interactions [9]. While the honeycomb lattice is not inherently frustrated, anisotropic interactions, parametrized by the Kitaev term (K), give rise to frustration between the competing orthogonal anisotropy axes. However, in real materials, the Kitaev interactions are often perturbed by Heisenberg interactions (J) giving rise to the strongly frustrated Heisenberg-Kitaev (J–K) model [10, 11].

Bond-dependent interactions stem from strong spin-orbit coupling in magnetic insulators. Hence heavy $4d$ and $5d$ transition metal ions have been proposed as a paradigm to realize a Kitaev QSL [12, 13]. Spin-orbit $J_{\text{eff}} = 1/2$ Mott insulators comprising low-spin d^5 and d^7 transition metal ions, such as Na_2IrO_3, $H_3LiIr_2O_6$, Li_2IrO_3, and $RuCl_3$ have been extensively studied to search for Kitaev physics [14–20]. An alternative approach is to explore $J_{\text{eff}} = 1/2$ magnetic moments from f-element ions, which exhibit significant anisotropy [21, 22]. In the $4f$ electron manifold, several electron configurations can host $J_{\text{eff}} = 1/2$ magnetic moments, with the one electron/one-hole ($4f^1/4f^{13}$) configurations as the most desirable. The one hole case is realized by the $J_{\text{eff}} = 1/2$ honeycomb material $YbCl_3$, the collective behavior of which was recently shown to be best described from the Heisenberg limit [23]. The one electron case leads to the $4f^1$ ions Ce^{3+} or Pr^{4+} including Na_2PrO_3, a material with edge sharing PrO_6 octahedra forming a honeycomb network similar to the iridates and recently proposed to exhibit dominant antiferromagnetic Kitaev interactions, contrasting with $4d$ and $5d$ systems [24].

In this work, the magnetic properties of Na_2PrO_3 are investigated using a combination of thermomagnetic and neutron scattering measurements on powder samples. These studies uncover spin-wave-like excitations at energies below 2 meV. A comparison to the isostructural compounds Na_2TbO_3 and Na_2CeO_3, that represent spin-only magnetic-moment and non-magnetic analogues of the title compound, respectively, yield deeper insights into the effective magnetic Hamiltonian of Na_2PrO_3. Although no magnetic Bragg peaks are observed within experimental sensitivity below the $T_N \approx 4.6$ K transition seen in thermomagnetic probes, dynamic correlations in Na_2PrO_3 are well explained by a model including antiferromagnetic nearest-neighbor interactions and a easy-axis XXZ exchange anisotropy. The inelastic data does not support the presence of a sizeable Kitaev term K. These studies also reveal an unusually small effective magnetic moment for the Pr^{4+} ions which is explained by the increased crystal-field splitting in comparison to trivalent lanthanides [25, 26].

Polycrystalline samples of $Na_2Ln^{4+}O_3$ with Ln = Ce ($4f^0$), Pr ($4f^1$), Tb ($4f^7$) were synthesized by solid-state reactions and structurally characterized by synchrotron x-ray diffraction [see [27] Sec. S1 and ref. [28]]. Na_2PrO_3 contains layers of PrO_6 octahedra forming distorted hon-

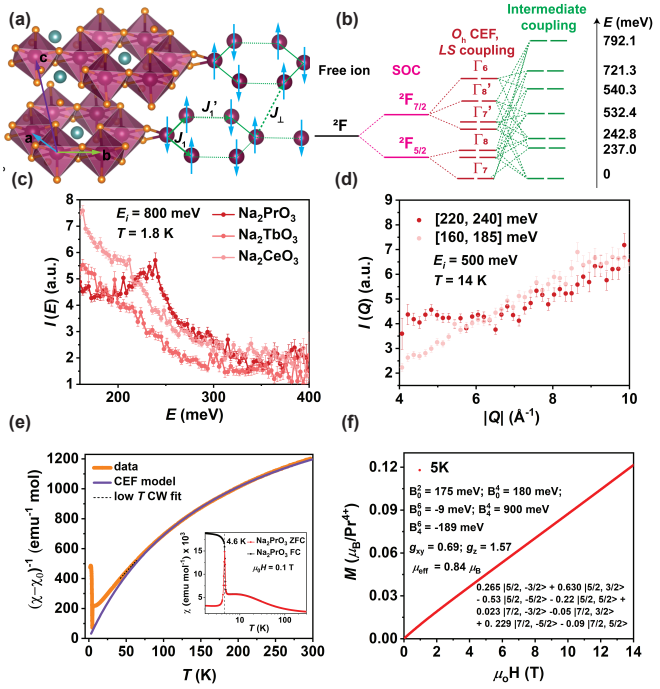


FIG. 1. (a) Monoclinic crystal structure of Na_2PrO_3 showing the honeycomb layers of Pr^{4+} ions and the resulting nearest neighbor and out-of-plane magnetic exchange pathways. (b) Comparison of the expected splitting of the $^2F_{5/2}$ free-ion ground-state of Pr^{4+} by SOC and a O_h CEF environment in LS and intermediate coupling. (c) Comparison between low momentum-transfer $Q \leq 6$ Å^{-1} inelastic neutron scattering spectra measured with $E_i = 800$ meV for Na_2LnO_3 (Ln = Ce, Pr, Tb) at $T = 1.8$ K. (d) Momentum-transfer dependence of the $E = 233(1)$ meV excitation at $T = 14$ K compared to phonon background at comparable energies. (e) The inverse magnetic susceptibility $1/(\chi(T)-\chi_0)$ and susceptibility $\chi(T)$ of Na_2PrO_3 in a 0.1 T field and $\chi_0 = 1.09\times10^{-3}$ emu mole^{-1}. The bold solid line (purple) is the CEF comparison to the data with the parameters of panel (f). The black and red traces in the inset corresponds to field-cooled (FC) and zero-field cooled measurements, respectively. (f) Isothermal magnetization $M(H)$ at $T = 5$ K and obtained CEF parameters.

eycomb networks separated by layers of Na ions, with two intraplane Pr–Pr distances $d = 3.407(3)$ Å and $d' = 3.487(6)$ Å, and an inter-plane distance of $d_\perp \approx 5.8$ Å at $T = 100$ K [Fig. 1(a)]. The ABC stacking sequence in the $C2/c$ space group originates from symmetry breaking displacements of the Na atoms which also lead to evident stacking faults in diffraction patterns. Na_2CeO_3 and Na_2TbO_3 are isostructural to Na_2PrO_3 [28]. Given the air-sensitivity of these samples, all synthesis and measurement operations where performed in an inert-gas atmosphere.

To understand the single-ion properties of Na_2PrO_3, broadband inelastic neutron scattering measurements on the fine-resolution Fermi chopper spectrometer (SEQUOIA) [29, 30] were performed at the Spallation Neutron Source (SNS), Oak Ridge National Laboratory (ORNL). Experiments were performed on ($m = 8$ g) polycrystalline samples loaded in annular Al powder cans and inserted into a liquid ^{4}He cryostat reaching a base temperature of $T = 1.5$ K. The data was reduced in MANTID [31] to yield the neutron scattering intensity $I(Q, E)$ as a function of momentum-transfer Q and energy-transfer E. We used a series of incoming energies to probe possible crystal electric field (CEF) excitations of our samples up to an energy transfer of $E \approx 800$ meV [see[27] Sec. S2 and refs. [32, 33]].

Pr^{4+} is a $4f^1$ Kramers ion, isoelectronic to Ce^{3+}, with a $^2F_{5/2}$ free-ion ground-state. For an octahedral oxygen environment with O_h symmetry, the CEF splitting leads to a Kramers doublet ground-state (Γ_7) and an excited quartet (Γ_8) which we expect to split into two doublets given the lower D_{2d} site-symmetry of Pr^{4+} in Na_2PrO_3 [Fig. 1(b)]. The energy-dependence of the neutron scattering intensity at low momentum-transfer $I(Q \leq 6$ Å$^{-1}, E)$ was used to search for these CEF excitations. The comparison of different E_i's and samples [Fig. 1(c) and SI Sec. S2] reveals a strong excitation at $E = 233(1)$ meV. The intensity of the excitation increases at low Q as expected for magnetic scattering [Fig. 1(d)]. The excitation found in Na_2PrO_3 compares well to the 260 meV Γ_7 to Γ_8 splitting observed for $BaPrO_3$ [34] which comprises Pr^{4+} ions in an ideal O_h environment. Since no other CEF excitations are observed below 500 meV, the $E = 233$ meV mode is associated with the two quasi-degenerate Γ_8 doublets [See [27] Sec. S2].

Given the axial distortion of the PrO_6 octahedra [See [27] Sec. S3 and refs. [35–37]], the CEF Hamiltonian can be written using the Wybourne tensor operators [36] as $\hat{\mathcal{H}}_{\rm CEF} = B_0^2\hat{C}_0^2 + B_0^4\hat{C}_0^4 + B_4^4\hat{C}_4^4 + B_0^6\hat{C}_0^6 + B_4^6\hat{C}_4^6$. The large CEF energy scale in Na_2PrO_3 has been observed indirectly by O K-edge X-ray absorption near edge spectroscopy studies of PrO_2 [26], and is similar in magnitude to the spin-orbit interaction $\lambda \approx 100$ meV resulting in a $\approx$ 360 meV separation between $^2F_{5/2}$ and $^2F_{7/2}$ for a free Pr^{4+} ion [38]. As a result, a mixing of the $^2F_{5/2}$ and $^2F_{7/2}$ electronic manifolds is expected and the above Hamiltonian must be diagonalized using the complete set of intermediate-coupling basis states using SPECTRE [39].

Given the number of CEF parameters, it is not possible to constrain the Hamiltonian solely using the observed excitation. To progress, it is possible to additionally match the temperature-dependence of the magnetic susceptibility for $\mu_0 H = 0.1$ T [Fig. 1(e)] and $T \geq 60$ K using the set of CEF parameters of Fig. 1(f) and a temperature independent term $\chi_0 = 1.09\times10^{-3}$ emu.mol^{-1}, although the CEF parameters remain under-constrained. The value of χ_0 is in reasonable agreement with the estimated value [40] $\chi_0 \approx \frac{8}{3\lambda}\mu_B^2 N_A = 0.8\times10^{-3}$ emu.mol^{-1} for a Pr^{4+} ion and with observations for the related com-

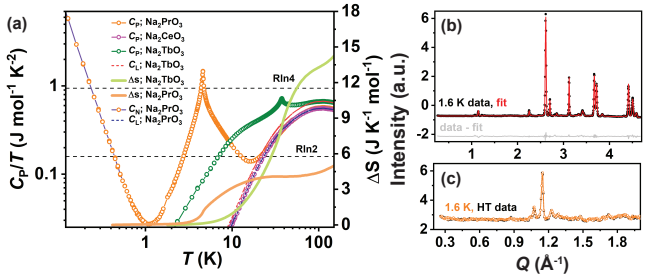


FIG. 2. (a) Heat capacity measurments of our $Na_2Ln^{4+}O_3$ samples measured using the relaxation method above T = 2 K. For Na_2PrO_3, measurements down to T = 100 mK were carried out using a dilution refrigerator insert on pressed pellets mixed with Ag. The change in magnetic entropy for Na_2PrO_3 and Na_2TbO_3 is obtained after subtracting the (scaled) lattice contribution from Na_2CeO_3. (b) Neutron diffration measurements on Na_2PrO_3 at T = 1.6 K using λ = 2.4 Å. The red line is the result from a Rietveld refinement. (Inset) Comparison at low-angle diffraction between T = 1.6 K and T = 55 K.

pound $BaPrO_3$ [41]. We note that a constrained form of the Hamiltonian preserving the proximate O_h crystal field symmetry with axial distortion as a perturbation does not allow to match the magnetic susceptibility [See [27] Sec. S4]. This choice of CEF parameters yields a ground-state doublet dominated by $|^2F_{5/2}, \pm 3/2\rangle$ and $|^2F_{7/2}, \pm 5/2\rangle$ states and predicts several higher-energy doublets beyond the 800 meV reach of our experiments [see [27] Sec. S2]. This also yields a calculated powder-averaged $g = 0.98$ for effective $J_{\rm eff} = 1/2$. The effective moment $\mu^{\rm eff}_{\rm CEF} = 0.84\ \mu_{\rm B}$/Pr is unusually small given the free-ion value is $\mu^{\rm free}_{\rm eff} = 2.54\mu_{\rm B}$/Pr. The small g-tensor is evident from the experimental isothermal magnetization at T = 5 K, which is linear and reaches only $\approx 0.12\ \mu_{\rm B}$/Pr at $\mu_0 H$ = 14 T, far short of saturation [Fig. 1(f)].

Below $T \approx 40$ K, the susceptibility of Na_2PrO_3 deviates from the single-ion form and culminates in a magnetic transition at T_N = 4.6 K, consistent with Ref. 42, with a clear splitting between field-cooled (FC) and zero-field cooled (ZFC) traces but no visible frequency dependence in ac susceptibility [See [27] Sec. S4]. Thus, this sharp peak is interpreted as magnetic ordering preceded by short-range order [Fig. 1(e)]. It is difficult to find an adequate regime for a Curie-Weiss analysis: a fit limited to $40 \le T \le 60$ K yields an antiferromagnetic Weiss constant $\Theta_{\rm W} = -30.4(1)$ K and $\mu^{\rm eff}_{\rm CW} = 1.19(1)\mu_{\rm B}$/Pr, comparable to $\mu^{\rm eff}_{\rm CEF}$. Heat capacity measurements [See [27] Sec. S5 and refs. [43, 44]] corroborate this picture [Fig. 2(a)]. An additional upturn is observed below T = 0.3 K, which is associated with nuclear spins. Subtracting the lattice contribution reveals an entropy change $\Delta S \approx 0.76R \ln 2$ between 0.1 K and 40 K, corroborating the $J_{\rm eff} = 1/2$ picture for Pr^{4+} and revealing some missing entropy.

To understand the ground-state of Na_2PrO_3 below the transition, neutron powder diffraction experiments were performed on the HB2A diffractometer [47] at the High Flux Isotope Reactor (HFIR), ORNL. No additional Bragg peaks are observed beyond the $C2/c$ nuclear structure [Fig. 2(b)], even after subtracting a T = 55 K background [Fig. 2(c). Given the high incoherent scattering background from the sample [See [27] Sec. S2], the small effective moment of Pr^{4+}, the stacking faults in the crystal structure, and the likelihood of a $\boldsymbol{k}_{\rm m} = 0$ propagation vector, this result is not entirely surprising. To get an estimate on any ordered moment $\langle \mu^z \rangle$, the hyperfine coupling in the nuclear specific-heat was modeled using a Schottky form. Assuming the entire upturn is nuclear yields a static electronic moment $\langle \mu^z_{\rm hyp} \rangle = 0.41\mu_{\rm B}$ at the time-scale of the nuclear-lattice relaxation [48], which is comparable to $\langle \mu^z_{\rm CEF} \rangle = 0.49\ \mu_{\rm B}$ estimated from CEF calculations.

In the absence of visible magnetic Bragg peaks in Na_2PrO_3, low-energy inelastic neutron scattering (E_i = 8, 20 meV) was employed to search for magnetic fluctuations. It is instructive to compare these results to the isostructural spin-only compound, Na_2TbO_3 [Fig. 3(a–e)]. Na_2TbO_3 orders at $T'_{\rm N} = 38.2$ K and develops structured spin-wave excitations below $T'_{\rm N}$ [Fig. 3(a,b)] with a band-top of 5 meV and a $\approx$ 1 meV gap. Inspecting the elastic line, and subtracting T = 55 K data from T = 20 K, evidences intense magnetic Bragg peaks indexed by a $\boldsymbol{k}_{\rm m} = 0$ propagation vector [Fig. 3(d)]. Representation analysis in SARAH [49] yields four possible magnetic structures, only one of which yields a good fit following a Rietveld refinement in FULLPROF [50] [See [27] Sec. S6]. Spins in the resulting Néel ordered structure lie in the ac-plane, essentially along c. Spin-wave excitations in Na_2TbO_3 are very intense given $S = 7/2$ [Fig. 3(e)] and can be efficiently modeled using linear spin-wave theory [51] in SPINW [52]. A spin Hamiltonian $\mathcal{H} = \mathcal{H}_{\rm ex} + D\sum_i (S^z_i)^2$ with Heisenberg exchange interactions J_1 and J'_1 for the split nearest-neighbor pairs (d and d'), $J_\perp$ between inequivalent lanthanide sites in two adjacent honeycomb planes, and a single-ion anisotropy term D is considered. The calculated powder-averaged intensity is in excellent agreement with the data [Fig. 3(c)] with parameters obtained after a grid-calculation and subsequent search for a minimal χ^2 [See [27] Sec. S7]. These parameters, $J_1 = 0.50$ meV, $J'_1 = 0.85J_1$, $J_\perp = -0.02J_1$ and $D = -0.001J_1$, indicate that the observed band-top dispersion [Fig. 3(a,b)] is induced by the splitting of J_1 and J'_1, and that the small spin gap is the combined effect of ferromagnetic $J_\perp$ and easy-axis D.

This forgoing analysis facilitates the description of the magnetic fluctuations in Na_2PrO_3 at T = 1.5 K [Fig. 3(f–i)], which resemble the spin-wave excitations in Na_2TbO_3 [Fig. 3(a)], but with a reduced band-top of 2 meV [Fig. 3(f)] and a scattering intensity decreased by a factor $\approx$ 30 [Fig. 3(b,f)]. Thus, a high temperature subtraction (T = 55 K) was utilized [Fig. 3(f)]. Given

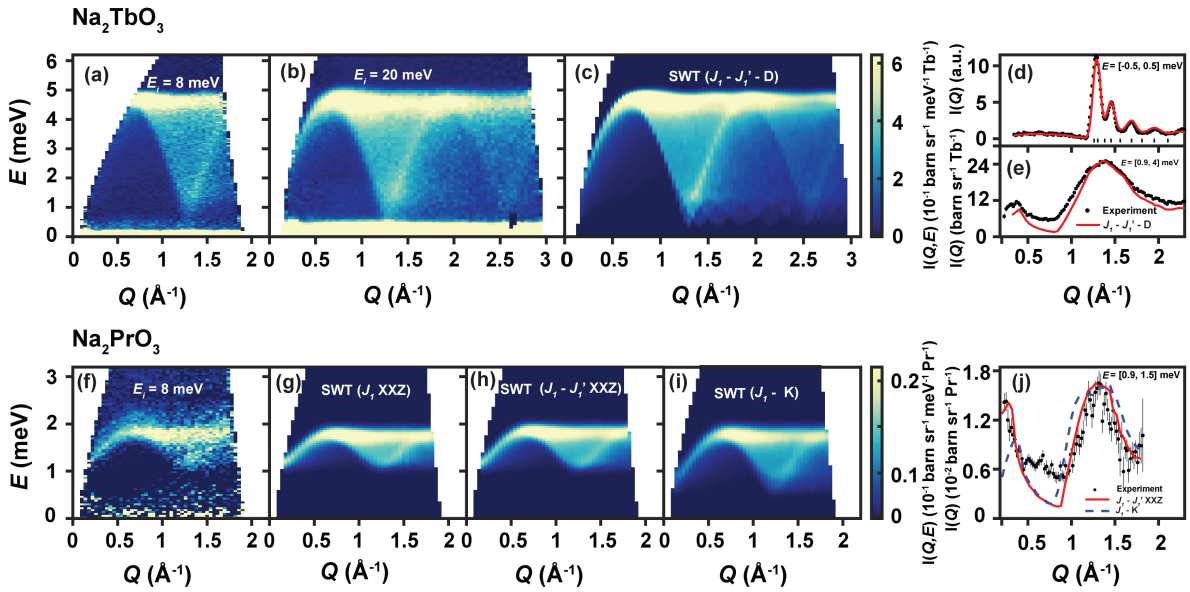


FIG. 3. (a-e) Inelastic neutron scattering intensity $I(Q, E)$ from Na_2TbO_3 at $T = 1.5$ K using (a) $E_i = 8$ meV or (b) $E_i = 20$ meV, where (b) is normalized to absolute units using the nuclear elastic scattering intensity [See [27] Sec. S9 and refs. [45, 46]] (c) Comparison with powder-averaged linear spin-wave theory calculations for optimized parameters including the magnetic form factor of Tb^{3+} and a constant energy energy broadening factor of 0.2 meV. The intensity in (a) was multiplied by a factor 0.25 to match the scale of (b-c). (d) Elastic magnetic scattering $-0.5 \leq E \leq 0.5$ meV of Na_2TbO_3 obtained by subtracting $T = 55$ K data from $T = 20$ K (black dots). The red line and vertical black ticks are the result of a Rietveld refinement using a $\boldsymbol{k}_m = 0$ propagation vector. (e) Momentum dependence of the low-energy inelastic signal $0.9 \leq E \leq 4$ meV (black dots) and comparison to linear spin-wave-theory predictions for optimized parameters (red line). (f-j) Inelastic neutron scattering results from Na_2PrO_3 at $T = 1.5$ K using (f) $E_i = 8$ meV, $T = 55$ K subtracted, and normalized to the absolute units. Comparison to linear spin-wave-theory predictions with optimized parameters for (g) a J_1 XXZ model with $\Delta = 1.22$ ($J_1 = 1.06$ meV), (h) a J_1–J_1' XXZ model with $\Delta = 1.26$ and $J_1' = 0.85J_1$ ($J_1 = 1.1$ meV), and (i) a J_1–K model with $K = 0.18J_1$ ($J_1 = 1.1$ meV). (i) Momentum dependence of the low-energy inelastic signal $0.9 \leq E \leq 1.4$ meV (black dots) and comparison to linear spin-wave-theory predictions for optimized parameters from the J_1–J_1' XXZ (solid red line) and J_1–K models (dashed blue line). To avoid over subtraction, the cut is taken from empty cryostat subtracted data while (f) shows a temperature subtracted spectrum.

that no static magnetic scattering is observed, an incipient $\boldsymbol{k}_m = 0$ order is assumed by analogy with Na_2TbO_3. Given the $J_{\text{eff}} = 1/2$ magnetic moments, several models are adopted to incorporate exchange anisotropies (scaled to the corresponding primary exchange) on J_1 and J_1' bonds, with spin-wave theory calculations performed in SPINW [See [27] Sec. S8]. Including a diagonal exchange anisotropy (XXZ), *e.g.* $\mathcal{H}_{\text{ex}} \equiv J \sum_{ij} (S_i^x S_j^x + S_i^y S_j^y + \Delta S_i^z S_j^z)$, opens a gap in the spectrum and yields an excellent agreement with the data for $J_1 = J_1' = 1.06$ meV and $\Delta = 1.22$ [Fig. 3(g)]. Allowing J_1' to vary independently slightly broadens the bandwidth but does not significantly improve the agreement between data and calculations [Fig. 3(h)]. Introducing a Kitaev term K in the Hamiltonian yields an overall agreement with the data for $J_1 = 1.1$ meV ($J_1' = J_1$) and an antiferromagnetic $K = 0.18J_1$, but introduces a weak double-gap feature at the band bottom that is clearly not observed in the experiment [Fig. 3(i)]. A cut through the low-energy part of the data and the corresponding spin-wave calculations [Fig. 3(j)] shows overall agreement, except between $Q = 0.25$ Å^{-1} and 1 Å^{-1} where background contributions are large. All models fail to account for the apparent continuum at the top of the band [See [27] Sec. S8], which we attribute to the presence of quantum fluctuations given recent studies on the honeycomb magnets $YbCl_3$ and $YbBr_3$ [23, 53]. Although single-crystal studies will be necessary to determine the relative importance of these terms in detail.

In conclusion, the 1.1(1) meV energy scale of the Heisenberg exchange interaction in Na_2PrO_3 is surprisingly large for a lanthanide system, that is reflected in the unusually large 230 meV scale of the crystal-electric field and the necessity to employ an intermediate-coupling scheme to explain the small effective moment per Pr^{4+}. Comparable CEF and SOC energy scales have also been proposed for $KCeO_2$ [54] and observed in $RuCl_3$ under pressure [55] where the impact of intermediate coupling on exchange was shown to favor antiferromagnetic Heisenberg interactions. Similar effects can hypothesized to be the origin of the considerably weaker antiferromagnetic Kitaev interaction, extracted by modeling the mag-

netic fluctuations of Na_2PrO_3, when compared to theoretical and *ab-initio* calculations [24]. The absence of visible magnetic Bragg peaks in Na_2PrO_3 as well as the missing entropy of around $0.3R\ln 2$ are two avenues for future inquiry. In particular, the observed low moment for the Pr^{4+} ion has important implications for the understanding and application of high-valence lanthanide ions in magnetic materials, since, akin to observations in high-valence actinides, this moment is derived from competition between SOC and CEF and necessitates the use of an intermediate coupling scheme to capture the observed temperature dependence [56, 57].

We thank Zhiling Dun for numerous helpful discussions and are indebted to Andrew Boothroyd for refining the definition of the Wybourne operators in an initial version of this manuscript. The work of A.R. and H.S.L. at Georgia Tech was supported by the Beckman Foundation as part of a Beckman Young Investigator Award to H.S.L. The work of M.D. and M.M. at Georgia Tech was supported by the National Science Foundation through grant NSF-DMR-1750186. This research used resources at the High Flux Isotope Reactor and Spallation Neutron Source, a DOE Office of Science User Facility operated by the Oak Ridge National Laboratory.

* These two authors contributed equally
† mourigal@gatech.edu
‡ hsl@gatech.edu

[1] L. Balents, Nature **464**, 199 (2010).
[2] C. Broholm, R. Cava, S. Kivelson, D. Nocera, M. Norman, and T. Senthil, Science **367** (2020).
[3] R. Sibille, E. Lhotel, V. Pomjakushin, C. Baines, T. Fennell, and M. Kenzelmann, Phys. Rev. Lett. **115**, 097202 (2015).
[4] K. Kimura, S. Nakatsuji, J. Wen, C. Broholm, M. Stone, E. Nishibori, and H. Sawa, Nat. Commun. **4**, 1934 (2013).
[5] J. A. Paddison, M. Daum, Z. Dun, G. Ehlers, Y. Liu, M. B. Stone, H. Zhou, and M. Mourigal, Nat. Phys. **13**, 117 (2017).
[6] M. M. Bordelon, E. Kenney, C. Liu, T. Hogan, L. Posthuma, M. Kavand, Y. Lyu, M. Sherwin, N. P. Butch, C. Brown, M. J. Graf, L. Balents, and S. D. Wilson, Nat. Phys. **15**, 1058 (2019).
[7] Z. Dun, X. Bai, J. A. Paddison, E. Hollingworth, N. P. Butch, C. D. Cruz, M. B. Stone, T. Hong, F. Demmel, M. Mourigal, and H. Zhou, Phys. Rev. X **10**, 031069 (2020).
[8] R. Sibille, N. Gauthier, E. Lhotel, V. Porée, V. Pomjakushin, R. A. Ewings, T. G. Perring, J. Ollivier, A. Wildes, C. Ritter, T. C. Hansen, D. A. Keen, G. J. Nilsen, L. Keller, S. Petit, and T. Fennell, Nat. Phys. **16**, 546 (2020).
[9] A. Kitaev, Ann. Phys. **321**, 2 (2006).
[10] J. Chaloupka, G. Jackeli, and G. Khaliullin, Phys. Rev. Lett **105**, 027204 (2010).
[11] Y. Singh, S. Manni, J. Reuther, T. Berlijn, R. Thomale, W. Ku, S. Trebst, and P. Gegenwart, Phys. Rev. Lett. **108**, 127203 (2012).
[12] Y. Motome, R. Sano, S. Jang, Y. Sugita, and Y. Kato, J. Phys.: Condens. Matter (2020).
[13] H. Takagi, T. Takayama, G. Jackeli, G. Khaliullin, and S. E. Nagler, Nat. Rev. Phys. (2019).
[14] A. Banerjee, C. Bridges, J.-Q. Yan, A. Aczel, L. Li, M. Stone, G. Granroth, M. Lumsden, Y. Yiu, and J. Knolle, Nat. Mater. **15**, 733 (2016).
[15] A. Banerjee, J. Yan, J. Knolle, C. A. Bridges, M. B. Stone, M. D. Lumsden, D. G. Mandrus, D. A. Tennant, R. Moessner, and S. E. Nagler, Science **356**, 1055 (2017).
[16] S. Choi, R. Coldea, A. Kolmogorov, T. Lancaster, I. Mazin, S. Blundell, P. Radaelli, Y. Singh, P. Gegenwart, and K. Choi, Phys. Rev. Lett **108**, 127204 (2012).
[17] K. Kitagawa, T. Takayama, Y. Matsumoto, A. Kato, R. Takano, Y. Kishimoto, S. Bette, R. Dinnebier, G. Jackeli, and H. Takagi, Nature **554**, 341 (2018).
[18] T. Takayama, A. Kato, R. Dinnebier, J. Nuss, H. Kono, L. Veiga, G. Fabbris, D. Haskel, and H. Takagi, Phys. Rev. Lett. **114**, 077202 (2015).
[19] R. Sano, Y. Kato, and Y. Motome, Phys. Rev. B **97**, 014408 (2018).
[20] H. Liu and G. Khaliullin, Phys. Rev. B **97**, 014407 (2018).
[21] F.-Y. Li, Y.-D. Li, Y. Yu, A. Paramekanti, and G. Chen, Phys. Rev. B **95**, 085132 (2017).
[22] J. G. Rau and M. J. Gingras, Phys. Rev. B **98**, 054408 (2018).
[23] G. Sala, M. B. Stone, B. K. Rai, A. F. May, P. Laurell, V. O. Garlea, N. P. Butch, M. D. Lumsden, G. Ehlers, G. Pokharel, A. Podlesnyak, D. Mandrus, D. S. Parker, S. Okamoto, B. G. Halasz, and A. D. Christianson, Nat. Commun. **12**, 1 (2021).
[24] S.-H. Jang, R. Sano, Y. Kato, and Y. Motome, Phys. Rev. B **99**, 241106 (2019).
[25] T. P. Gompa, A. Ramanathan, N. T. Rice, and H. S. La Pierre, Dalton Trans. **49**, 15945 (2020).
[26] S. G. Minasian, E. R. Batista, C. H. Booth, D. L. Clark, J. M. Keith, S. A. Kozimor, W. W. Lukens, R. L. Martin, D. K. Shuh, S. C. E. Stieber, T. Tylisczcak, and X.-d. Wen, J. Am. Chem. Soc. **139**, 18052 (2017).
[27] See Supplemental Material at [URL] for sample preparation, INS, ac susceptibility, specific heat and spin wave analysis.
[28] A. Ramanathan, J. E. Leisen, and H. S. La Pierre, Inorg. Chem. **60**, 1398 (2021).
[29] G. E. Granroth, A. I. Kolesnikov, T. E. Sherline, J. P. Clancy, K. A. Ross, J. P. C. Ruff, B. D. Gaulin, and S. E. Nagler, J. Phys.: Conf. Series **251**, 012058 (2010).
[30] M. B. Stone, J. L. Niedziela, D. L. Abernathy, L. DeBeer-Schmitt, G. Ehlers, O. Garlea, G. E. Granroth, M. Graves-Brook, A. I. Kolesnikov, A. Podlesnyak, and B. Winn, Rev. Sci. Instrum. **85**, 045113 (2014).
[31] O. Arnold, J. Bilheux, J. Borreguero, A. Buts, S. Campbell, L. Chapon, M. Doucet, N. Draper, R. F. Leal, M. Gigg, V. Lynch, A. Markvardsen, D. Mikkelson, R. Mikkelson, R. Miller, K. Palmen, P. Parker, G. Passos, T. Perring, P. Peterson, S. Ren, M. Reuter, A. Savici, J. Taylor, R. Taylor, R. Tolchenov, W. Zhou, and J. Zikovsky, Nucl. Instrum. Methods Phys. Res., Sect. A **764**, 156 (2014).
[32] C.-K. Loong, L. Iton, and M. Ozawa, Physica B: Condensed Matter **213**, 640 (1995).

[33] R. Senesi, D. Flammini, A. I. Kolesnikov, É. D. Murray, G. Galli, and C. Andreani, The Journal of chemical physics **139**, 074504 (2013).

[34] S. Kern, C.-K. Loong, and G. H. Lander, Phys. Rev. B **32**, 3051 (1985).

[35] U. Walter, Journal of Physics and Chemistry of Solids **45**, 401 (1984).

[36] B. G. Wybourne, (1965).

[37] V. Kaufman and J. Sugar, Journal of research of the National Bureau of Standards. Section A, Physics and chemistry **71**, 583 (1967).

[38] Y. Hinatsu and N. Edelstein, J. Solid State Chem. **112**, 53 (1994).

[39] A. Boothroyd, "Spectre, a program for calculating spectroscopic properties of rare earth ions in crystals(1990–2014),".

[40] J. Chaloupka, G. Jackeli, and G. Khaliullin, Phys. Rev. Lett **110**, 097204 (2013).

[41] M. Bickel, G. Goodman, L. Soderholm, and B. Kanellakopulos, J. Solid State Chem. **76**, 178 (1988).

[42] Y. Hinatsu and Y. Doi, J. Alloys Compd. **418**, 155 (2006).

[43] B. Bleaney, Handbook on the Physics and Chemistry of rare earths **11**, 323 (1988).

[44] R. J. Elliott and K. Stevens, Proceedings of the Royal Society of London. Series A. Mathematical and Physical Sciences **218**, 553 (1953).

[45] J. A. Paddison, H. S. Ong, J. O. Hamp, P. Mukherjee, X. Bai, M. G. Tucker, N. P. Butch, C. Castelnovo, M. Mourigal, and S. Dutton, Nat. commun. **7**, 1 (2016).

[46] M. Mourigal, W. Fuhrman, J. Sheckelton, A. Wartelle, J. Rodriguez-Rivera, D. L. Abernathy, T. McQueen, and C. L. Broholm, Phys. Rev. Lett **112**, 027202 (2014).

[47] V. O. Garlea, B. C. Chakoumakos, S. A. Moore, G. B. Taylor, T. Chae, R. G. Maples, R. A. Riedel, G. W. Lynn, and D. L. Selby, Appl. Phys. A **99**, 531 (2010).

[48] K. Kimura, S. Nakatsuji, J. Wen, C. Broholm, M. Stone, E. Nishibori, and H. Sawa, Nat. commun. **4**, 1 (2013).

[49] A. S. Wills, Phys. B (Amsterdam, Neth.) **276–278**, 680 (2000).

[50] J. Rodríguez-Carvajal, Phys. B (Amsterdam, Neth.) **192**, 55 (1993).

[51] S. Petit, Collection SFN **12**, 105 (2011).

[52] S. Toth and B. Lake, J. Phys.: Condens. Matter **27**, 166002 (2015).

[53] C. Wessler, B. Roessli, K. W. Krämer, B. Delley, O. Waldmann, L. Keller, D. Cheptiakov, H. B. Braun, and M. Kenzelmann, npj quantum materials **5**, 1 (2020).

[54] M. S. Eldeeb, T. Petersen, L. Hozoi, V. Yushankhai, and U. K. Rößler, Phys. Rev. Materials **4**, 124001 (2020).

[55] G. Bastien, G. Garbarino, R. Yadav, F. J. Martinez-Casado, R. Beltrán Rodríguez, Q. Stahl, M. Kusch, S. P. Limandri, R. Ray, P. Lampen-Kelley, D. G. Mandrus, S. E. Nagler, M. Roslova, A. Isaeva, T. Doert, L. Hozoi, A. U. B. Wolter, B. Büchner, J. Geck, and J. van den Brink, Phys. Rev. B **97**, 241108 (2018).

[56] N. Magnani, P. Santini, G. Amoretti, and R. Caciuffo, Phys. Rev. B **71**, 054405 (2005).

[57] L. Escalera-Moreno, J. J. Baldoví, A. Gaita-Ariño, and E. Coronado, Inorg. Chem. **58**, 11883 (2019).